*Inorg. Chem.* **2004**, *43*, 173–180


# Preparation, Characterization, and Condensation of Copper Tellurolate Clusters in the Pores of Periodic Mesoporous Silica MCM-41

**Collin M. Kowalchuk,[†] GUnter Schmid,[‡] Wolfgang Meyer-Zaika,[‡] Yining Huang,*[,†] and John F. Corrigan*[,†]**

*Department of Chemistry, The University of Western Ontario, London Ontario, N6A 5B7 Canada, and Institut für Anorganische Chemie, Universität Essen, Essen, D-45177 Germany*

Received March 3, 2003

The copper–tellurolate cluster $[(Cu_6(TePh)_6(PPh_2Et)_5]$ has been loaded into the pores of MCM-41 by solid-state impregnation techniques. It was found that the best loading conditions are 110 °C and $10^{-3}$ Torr static vacuum. The resulting material was analyzed by powder X-ray diffraction (PXRD), nitrogen adsorption isotherms, thermogravimetric analysis (TGA), $^{31}$P CP MAS NMR spectroscopy, and TEM. It was observed that loading is accompanied by loss of the phosphine shell, with retention of the copper–tellurium core. Condensation of the impregnated material may proceed thermally or photochemically. Thermal condensation results in the formation of $Cu_2Te$ nanoparticles as demonstrated by PXRD, and TEM data suggests that the process has taken place inside the pores of MCM-41. Photochemical condensation yields larger metal–chalcogen clusters in the pores as suggested by the result of UV–vis diffuse reflectance spectroscopy and TEM measurements.

## Introduction

Transition metal−chalcogenide particles with nanoscale dimensions have received much attention due to the interesting physical properties exhibited by these "small pieces of solids".[1] Among these, reports detailing the synthesis of nanocrystalline copper−telluride are relatively few,[2−5] due primarily to handling difficulties of Te precursors.[6] The preparation of $Cu_2Te$ nanoparticles and nanorods from elemental tellurium and copper salts using microwave heating[2] and redox methods,[3] respectively, has been described. Copper−tellurolate (CuTeR) clusters represent a convienent "premixed" precursor to copper−telluride due to the well-established tellurolate−telluride decompostition pathway:[7,8]

$$M(TeR)_2 \xrightarrow{\Delta} MTe + 0.5TeR_2$$

From this perspective, and due to the ease of handling of polynuclear Cu−TeR complexes,[9,10] the controlled decomposition of copper−tellurolates into solid copper−telluride presents a viable route to this semiconductor. Thermal condensation of such complexes within the size restricting

* Authors to whom correspondence should be addressed. E-mail: corrigan@uwo.ca (J.F.C.); yhuang@uwo.ca (Y.H.).
[†] The University of Western Ontario.
[‡] Universität Essen.

(1) (a) Henglein, A. *Chem. Rev.* **1989**, *89*, 1861. (b) Weller, H. *Angew. Chem., Int. Ed. Engl.* **1993**, *32*, 41. (c) Alivisatos, A. P. *J. Phys. Chem.* **1996**, *100*, 13226.
(2) (a) Palchik, O.; Kerner, R.; Zhu, Z.; Gedanken, A. *J. Solid State Chem.* **2000**, *154*, 530. (b) Zhang, Y.; Qiao, Z.-P.; Chen, X.-M. *J. Mater. Chem.* **2002**, *12*, 2747.
(3) Jiang, Y.; Xie, B.; Wu, J.; Yuan, S.; Wu, Y.; Huang, H.; Qian, Y. *J. Solid State Chem.* **2002**, *167*, 28.
(4) (a) Henshaw, G.; Parkin, I. P.; Shaw, G. A. *J. Chem. Soc., Dalton Trans.* **1997**, 231. (b) Yang, J.; Yu, S.-H.; Han, Z.-H.; Qian, Y. T.; Zhang, Y.-H. *J. Solid State Chem.* **1999**, *387−389*, 387.
(5) Sridhar, K.; Chattopadhyay, K. *J. Alloys Compd.* **1998**, *264*, 293.
(6) Roof, L. A.; Kolis, J. W. *Chem. Rev.* **1993**, *93*, 1037.
(7) (a) Brennan, J. G.; Siegrist, T.; Carroll, P. J.; Stuczynski, S. M.; Reynders, P.; Brus, L. E.; Steigerwald, M. L. *Chem. Mater.* **1990**, *2*, 403. (b) Christou, V.; Arnold, J. *J. Am. Chem. Soc.* **1992**, *114*, 6240. (c) Cary, D. R.; Arnold, J. *J. Am. Chem. Soc.* **1993**, *115*, 2520. (d) Seligson, A. L.; Arnold, J. *J. Am. Chem. Soc.* **1993**, *115*, 8214. (e) Cary, D. R.; Arnold, J. *Inorg. Chem.* **1994**, *33*, 1791. (f) Strzelecki, A. R.; Likar, C. L.; Helsel, B. A.; Utz, T.; Lin, M.; Bianconi, P. A. *Inorg. Chem.* **1994**, *33*, 5188. (g) Bochmann, M.; Bwembya, G. C.; Powell, A. K.; Song, X. *Polyhedron* **1995**, *14*, 3495.
(8) (a) Piers, W.; MacGillivray, L. R.; Zaworotko, M. *Organometallics* **1993**, *12*, 4723. (b) Piers, W. E.; Parks, D. J.; MacGillivray, L. R.; Zaworotko, M. J. *Organometallics* **1994**, *13*, 4547. (c) Gindelberger, D. E.; Arnold, J. *Organometallics* **1994**, *13*, 4462. (d) Knight, L. K.; Piers, W. E.; McDonald, R. *Chem.−Eur. J.* **2000**, *6*, 4322.
(9) Corrigan, J. F.; Fenske, D. *Angew. Chem., Int. Ed. Engl.* **1997**, *36*, 1981.
(10) (a) Fenske, D.; Corrigan, J. F. In *Metal Clusters in Chemistry*; Braunstein, P., Oro, L. A., Raithby, P. R., Eds.; Wiley-VCH: Weinheim, 1999; Vol. 3, p 1302. (b) DeGroot, M. W.; Cockburn, M. W.; Workentin, M. S.; Corrigan, J. F. *Inorg. Chem.* **2001**, *40*, 4678.

10.1021/ic0300868 CCC: $27.50 
Published on Web 12/06/2003

channels of a mesoporous host would allow for control of particle size. It has been shown that nanometer sized particles[11,12] and clusters[9,10,13] can be accessed from smaller metal−chalcogenolate complexes and these reactions also proceed via the elimination of $ER_2$ from $M(ER)_2$ centers (E = S, Se, and Te).[7,9,10,12,14] Condensation of metal chalcogenolate clusters may be photochemically induced or proceed through thermal processes, and it has been demonstrated that the photocondensation of $Cu_6(TePh)_6(PPh_2Et)_5$ **1** results in the layered structure $[Cu_{50}(TePh)_{20}Te_{17}(PEtPh_2)_8]^{4-}$.[9]

Mesoporous M41s silicates, first synthesized in 1992,[15] show promise for templating materials in the desired nanometer size regime due to a pore size which may be varied between 2 and 10 nm. The structure is fabricated primarily of tetrahedral $Q^4$ ($SiO_4$) species in a honeycomb one-dimensional array of nanotubules. Within the pores $Q^3$ ($O_3$-SiOH) groups provide the material with weak acidic properties[16] and act as sites for further functionalization of the pore wall.[15b,17]

Many studies have focused on exploring the nanochemistry within the pores of MCM-41. These include the formation of polyanaline filaments within the pores,[18] polymer fibers,[19] and the synthesis of main group, transition metal, and nonmetal nanofibers from molecular precursors.[20−25] Metal−pnictogenide,[26,27] metal,[28] metal−oxide,[29,30] and chalcogenide[31−34] nanoparticles have also been formed in the channels of the mesoporous host. ZnS/-, CdS/-, and CuS/MCM-41 binary nanoclusters have been prepared by solution loading a suitable organometallic precursor, followed by calcination and reaction with $H_2S$.[31] CdS nanoparticles have been incorporated[33] and diluted magnetic II−VI semiconductor nanoparticles have been synthesized within the pores.[34] All of these studies demonstrate the nanochemistry possible within MCM-41.

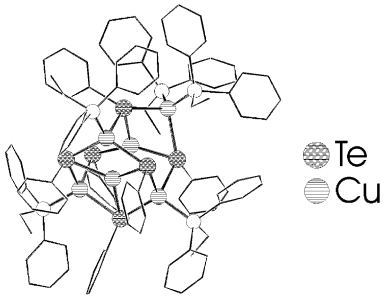


**1**

We recently reported the preliminary results on the occlusion of the copper−tellurolate complex, $Cu_6(TePh)_6(PPh_2Et)_5$ **1**, in the pores of MCM-41.[35] Herein, we present the

(11) Cumberland, S. L.; Hanif, K. M.; Javier, A.; Khitrov, G. A.; Strouse, G. F.; Woessner, S. M.; Yun, C. S. *Chem. Mater.* **2002**, *14*, 1576.
(12) (a) Babcock, J. R.; Zehner, R. W.; Sita, L. R. *Chem. Mater.* **1998**, *10*, 2027. (b) Bahr, S. R.; Boudjouk, P.; McCarthy, G. J. *Chem. Mater* **1992**, *4*, 383. (c) Jun, Y.-W.; Choi, C.-S.; Cheon, J. *Chem. Commun.* **2001**, 101.
(13) Tran, D. T. T.; Taylor, N. J.; Corrigan, J. F. *Angew. Chem., Int. Ed.* **2000**, *39*, 935.
(14) (a) Steigerwald, M. L.; Sprinkle, C. R. *J. Am. Chem. Soc.* **1987**, *109*, 7200. (b) Brennan, J. G.; Siegrist, T.; Carroll, P. J.; Stuczynski, S. M.; Brus, L. E.; Steigerwald, M. L. *J. Am. Chem. Soc.* **1989**, *111*, 4141. (c) Bochmann, M.; Webb, K.; Harman, M.; Hursthouse, M. B. *Angew. Chem., Int. Ed. Engl.* **1990**, *29*, 638. (d) Malik, M. A.; O'Brien, P. l. *Chem. Mater.* **1991**, *3*, 999. (e) Strzelecki, A. R.; Likar, C. L.; Helsel, B. A.; Utz, T.; Lin, M.; Bianconi, P. A. *Inorg. Chem.* **1994**, *33*, 5188. (f) O'Brien, P.; Nomura, R. *J. Mater. Chem.* **1995**, *5*, 1761. (g) Stoll, S. L.; Barron, A. R. *Chem. Mater.* **1998**, *10*, 650. (h) Chunggaze, M.; McAleese, J.; O'Brien, P.; Otway, D. J. *Chem. Commun.* **1998**, 833. (i) Lazell, M.; O'Brien, P.; Otway, D. J.; Park, J.-H. *J. Chem. Soc., Dalton Trans.* **2000**, 4479.
(15) (a) Kresge, C. T.; Leonowicz, M. E.; Roth, W. J.; Vatuli, J. C.; Beck, J. S. *Nature* **1992**, *359*, 710. (b) Beck, J. S.; Vartuli, J. C.; Roth, W. J.; Leonowicz, M. E.; Kresge, C. T.; Schmitt, K. D.; Chu, C. T.-W.; Olson, D. H.; Sheppard, E. W.; McCullen, S. B.; Higgins, J. B.; Schlenker, J. L. *J. Am. Chem. Soc.* **1992**, *114*, 10834.
(16) (a) Luan, Z.; Cheng, C.-F.; Zhou, W.; Klinowski, J. *J. Phys. Chem.* **1995**, *99*, 1018−1024. (b) Weglarski, J.; Datka, J.; He, H.; Klinowski, J. *J. Chem. Soc., Faraday Trans.* **1996**, *92*, 5161. (c) Jentys, A.; Kleestorfer, K.; Vinek, H.; *Microporous Mesoporous Mater.* **1999**, *27*, 321.
(17) (a) Sutra, P.; Fajula, F.; Brunel, D.; Lentz, P.; Daelen, G.; Nagy, J. B. *Colloids Surf.* **1999**, *158*, 21. (b) Brunel, D.; Cauvel, A.; Di Renzo, F.; Fajula, F.; Fubini, B.; Onida, B.; Garrone, E. *New J. Chem.* **2000**, *24*, 807.
(18) (a) Wu, C.-G.; Bein, T. *Science* **1994**, *264*, 1757. (b) Wu C.-G.; Bein, T. *Chem. Mater.* **1994**, *6*, 1109.
(19) (a) Johnson, S. A.; Khushalani, D.; Coombs, N.; Mallouk, T. E.; Ozin, G. A. *J. Mater. Chem.* **1998**, *8*, 13. (b) Jang, J.; Lim, B.; Lee, J.; Hyeon, T. *Chem. Commun.* **2001**, 83.
(20) Leon, R.; Margolese, D.; Stucky, G.; Petroff, P. M. *Phys. Rev. B* **1995**, *52* (4), 2285.
(21) (a) Ko, C. H.; Ryoo, R. *Chem. Commun.* **1996**, 2467. (b) Sasaki, M.; Osada, M.; Sugimoto, N.; Inagaki, S.; Fukushima, Y. Fukuoka, A.; Ichikawa, M. *Microporous Mesoporous Mater.* **1998**, *21*, 597. (c) Liu, Z.; Sakamoto, Y.; Ohsuna, T.; Hiraga, K.; Terasaki, O.; Ko, C. H.; Shin, H. J.; Ryoo, R. *Angew. Chem., Int. Ed.* **2000**, *39*, 3107.
(22) Fukuoka, A.; Sakamoto, Y.; Guan, S.; Inagaki, S.; Sugimoto, N.; Fukushima, Y.; Hirahara, K.; Iijima, S.; Ichikawa, M. *J. Am. Chem. Soc.* **2001**, *123*, 3373.
(23) Han, Y.-J.; Kim, J. M.; Stucky, G. D. *Chem. Mater.* **2000**, *12*, 2068.
(24) Coleman, N. R. B.; Morris, M. A.; Spalding, T. R.; Holmes, J. D. *J. Am. Chem. Soc.* **2001**, *123*, 187.
(25) Huang, M. H.; Choudrey, A.; Yang, P. *Chem. Commun.* **2000**, 1063.
(26) Agger, J. R.; Anderson, M. W.; Pemble, M. E.; Terasaki, O.; Nozue, Y. *J. Phys. Chem. B* **1998**, *102*, 3345.
(27) Srdanov, V. I.; Alxneit, I.; Stucky, G. D.; Reaves, C. M.; DenBaars, S. P. *J. Phys. Chem. B* **1998**, *102*, 3341.
(28) (a) MacLachlan, M. J.; Aroca, P.; Coombs, N.; Manners, I.; Ozin, G. A. *Adv. Mater.* **1998**, *10*, 144. (b) MacLachan, M. J.; Ginzburg, M.; Coombs, N.; Raju, N. P.; Greedan, J. E.; Ozin, G. A.; Manners, I. *J. Am. Chem. Soc.* **2000**, *122*, 3878.
(29) (a) Abe, T.; Tachibana, Y.; Uematsu, T.; Iwamoto, M. *J. Chem. Soc., Chem. Commun.* **1995**, 1617. (b) Moller, K.; Bein, T. *Chem. Mater.* **1998**, *10*, 2950. (c) Mulukutla, R. S.; Asakura, K.; Namba, S.; Iwasawa, Y. *Chem. Commun.* **1998**, 1425. (d) Mulukutla, R. S.; Asakura, K.; Kogure, T.; Namba, S.; Iwasawa, Y. *Phys. Chem. Chem. Phys.* **1999**, *1*, 2027−2032. (e) Zhang, W.-H.; Shi, J.-L.; Wang, L.-Z.; Yan, D.-S. *Chem. Mater.* **2000**, *12*, 1408.
(30) (a) Schmechel, R.; Kennedy, M.; von Seggern, H.; Winkler, H.; Kolbe, M.; Fischer, R. A.; Xaomao, L.; Benker, A.; Winterer, M.; Hahn, H. *J. Appl. Phys.* **2001**, *89*, 1679. (b) Chen, W.; Joly, A. G.; Kowalchuk, C. M.; Malm, J.-O.; Huang, Y.; Bovin, J.-O. *J. Phys. Chem. B* **2002**, *106*, 7034.
(31) Zhang, W.-H.; Shi, J.-L.; Chen, H.-R.; Hua, Z.-L.; Yan, D.-S. *Chem. Mater.* **2001**, *13* (2), 648.
(32) Parala, H.; Winkler, H.; Kolbe, M. Wohlfart, A.; Fischer, R. A.; Schmechel, R.; von Seggern, H. *Adv. Mater.* **2000**, *12* (14), 1050.
(33) (a) Hirai, T.; Okubo, H.; Komasawa, I. *J. Phys. Chem B* **1999**, *103*, 4228. (b) Hirai, T.; Okubo, H.; Komasawa, I. *J. Colloid Interface Sci.* **2001**, *235*, 358. (c) Zhang, Z.; Dai, S.; Fan, X.; Blom, D. A.; Pennycook, S. J.; Wei, Y. *J. Phys. Chem. B* **2001**, *105*, 6755. (d) Wellmann, H.; Rathousky, J.; Wark, M.; Zukal, A.; Schulz-Ekloff, G. *Microporous Mesoporous Mater* **2001**, *44*−*45*, 419. (e) Xu, W.; Liao, Y.; Akins, D. L. *J. Phys. Chem. B* **2002**, *106*, 11127. (f) Chae, W.-S.; Ko, J.-H.; Hwang, I.-W.; Kim, Y.-R. *Chem. Phys. Lett.* **2002**, *365*, 49.
(34) (a) Brieler, F. J.; Fröba, M.; Chen, L.; Klar, P. J.; Heimbrodt, W.; Krug von Nidda, H.-A.; Loidl, A. *Chem. Eur. J.* **2002**, *8*, 185. (b) Chen, L.; Falk, H.; Klar, P. J.; Heimbrodt, W.; Brieler, F.; Fröba, M.; Krug von Nidda, H.-A.; Loidl, A.; Chen, Z.; Oka, Y. *Phys. Status Solidi* **2002**, *229*, 31.

full details of the impregnation of **1** and subsequent thermal and photochemical condensation within the pores of MCM-41.

## Experimental Section

All manipulations were performed under an atmosphere of $N_2$, except where noted otherwise.

**Chemical Agents.** $Et_2O$ and sulfuric acid were purchased from EM science. THF, pentane, and hexanes were obtained from Caledon. All nonchlorinated solvents were dried using sodium with benzophenone as an indicator and distilled. $CH_2Cl_2$ was purchased from BDH and dried over $P_2O_5$. Cetyltrimethylammonium bromide and diphenylethyl phosphine oxide were purchased from Aldrich. N-brand sodium silicate (28.7% $SiO_2$) was obtained from the PQ corporation.

$Cu_6(TePh)_6(PPh_2Et)_5$ **1** was prepared according to the published procedure,[9] and its purity was confirmed via comparison of cell constants of single crystals with the published values. MCM-41 was synthesized under hydrothermal conditions according to literature procedures.[15] The $C_{16}$ surfactant (cetyltrimethylammonium bromide) was employed as a template which provides a pore size easily large enough to accommodate cluster **1**. MCM-41 was characterized by PXRD. PXRD *d* spacings (nm): 3.83 ($d_{100}$), 2.22 ($d_{110}$), 1.96 ($d_{200}$).

**Procedures. Loading Procedure.** A 0.20 g sample of MCM-41 was dehydrated in a Schlenk tube at 130 °C for 3 h in vacuo to remove adsorbed water from the MCM-41 sample, as determined by thermogravimetric analysis (TGA). In a glovebox, a specific mass of **1** (12−20 wt % compared to MCM-41) was added in crystalline form and the crystals were evenly distributed on the exterior of MCM-41 by mechanical mixing. Samples of **1**/MCM-41 were prepared by heating at 70 °C under dynamic vacuum ($10^{-3}$ Torr) (I) and 110 °C $10^{-3}$ Torr static vacuum (II) with a loading range of 12−20 wt %. The maximum loading of **1** into MCM-41 was found to be ∼30 wt %, however reproducibility was highest when loadings were between 12 and 20 wt %. TGA was used to monitor loading conditions as discussed in the Results and Discussion section. PXRD, nitrogen adsorption, TGA, $^{31}$P CP MAS NMR spectroscopy, and TEM were used to characterize the resulting samples. A control sample was prepared, where **1** only exists on the external surface, by combining 0.10 g of silicalite-1 (pore diameter 0.53 nm, dehydrated at 400 °C, $10^{-3}$ Torr) with 20 wt % of **1**. The sample (III) was heated at 70 °C, $10^{-3}$ Torr dynamic vacuum and analyzed by TGA.

$PPh_2Et$/MCM-41 complexes (IV) were prepared by dehydrating 0.20 g of MCM-41 and adding 20 wt % $PPh_2Et$. The mixture was then placed under $10^{-3}$ Torr static vacuum. Loading was achieved by heating the mixture at 110 °C for a period of 24 h. TGA and $^{31}$P CP MAS NMR experiments were then performed to characterize the samples.

$Ph_2EtPO$/MCM-41 samples (V) were prepared by combining 0.20 g of dehydrated MCM-41 with 20 wt % $PPh_2EtO$ in a glovebox. A volume of 15 mL of $CH_2Cl_2$ was added, and the suspension was stirred overnight. The solvent was then removed by vacuum. Heating for a period of 24 h at 110 °C under a reduced pressure of $10^{-3}$ Torr ensured even coverage of the $Ph_2EtPO$. The samples were analyzed by TGA and $^{31}$P CP MAS NMR spectroscopy.

Hydrogen analysis was performed on the evolved gas after the preparation of II. A sample of II was prepared from 0.20 g of MCM-41 and 0.04 g of **1** by treating at 110 °C, $10^{-3}$ Torr in a Schlenk tube directly attached to a vacuum line. After the loading procedure any volatiles produced were trapped in a separate Schlenk cooled in liquid $N_2$. While maintaining the cold trap a vessel of activated charcoal, also cooled in liquid $N_2$ was exposed to the residual gas evolved during the loading. The collected gas was analyzed by mass spectrometry for $H_2$.

**Thermolysis of II (12 Wt %).** Samples were loaded into a 70 $\mu$L Pt crucible (typically ≈0.03 g) and heated from 25 °C to the annealing temperature at a rate of 10 °C/min under a nitrogen flow of 70 mL/min in a thermogravimetric analyzer. Separate samples were annealed at 550, 750, or 950 °C for 30 min. The process was repeated until 0.1 g of material was obtained and analyzed by PXRD.

**Photolysis of II (12 Wt %).** Samples were loaded into a UV diffuse reflectance cell equipped with a quartz window. Irradiation was performed using a low pressure Hg lamp ($\lambda$ < 254 nm). Pure **1** was ground into a fine powder and diluted with KBr in a 1:4 ratio to obtain a useful reflectance scale. **1**/MCM-41 required no dilution before solid state photolysis. UV−vis diffuse reflectance spectra were obtained at regular time intervals. Photolysis was also carried out in a quartz Schlenk tube equipped with a stir bar. Slurries of 0.1 g of **1** and **1**/MCM-41 in hexane (in which **1** has low solubility) were irradiated for 6 h with stirring. The mother liquor was analyzed by GC/MS.

**Characterization.** Powder X-ray diffraction patterns were obtained on a Rigaku diffractometer with Co Kα radiation ($\lambda$ = 1.799260 Å). Calculations of the powder patterns for **1** were performed using the SHELXTL commercial software package (Bruker) utilizing the XPOW program with the single-crystal X-ray diffraction data.[9] Nitrogen adsorption data were obtained on a Micromeritics ASAP 2010 isotherm instrument. Prior to nitrogen adsorption measurements the calcined MCM-41 and **1**/MCM-41 complexes were outgassed at 106 °C to eliminate any water from the sample introduced during sample transfer without affecting loaded **1**. The samples were held at the outgas temperature overnight (>12 h). Samples were cooled to room temperature prior to adsorption measurement at 77 K. The BET surface area and the total pore volume were obtained using the Micromeritics ASAP V5.01 software. Thermogravimetric analyses were performed on a Mettler Toledo TGA/SDTA851$^e$ analyzer. TGA measurements were carried out with a dynamic temperature program of 25−550 °C or 25−750 °C with a heating rate 10 °C/min. SDTA measurements were obtained concurrently. The $^{31}$P cross polarization (cp) MAS spectra were obtained on a Varian/Chemagnetic Infinitypulse 400 wide bore spectrometer at the field strength of 9.4 T, with resonance frequencies of 399.491 and 161.719 MHz for $^1$H and $^{31}$P, respectively. A Varian/Chemagnetic 3.2-mm double tuned MAS probe was used. The rotor frequency was in the range of 14 to 18 kHz. $^{31}$P NMR spectra were referenced to 85% $H_3PO_4$ using $(NH_4)H_2PO_4$ as a secondary reference. The Hartmann−Hahn condition was determined using $(NH_4)H_2PO_4$. The proton 90° pulse length was typically 2 $\mu$s with an optimized contact time of 2 ms. The variable amplitude CP[36] and two pulse phase modulated (TPPM) decoupling[37] methods were utilized. The proton recycle delay for CP experiments was 5 s.

Hydrogen analysis was performed using a VG Prism-series, dual inlet mass spectrometer. EDX (energy dispersion X-ray) analysis was obtained on an EDAX Phoenix model EDX system with light

(35) (a) Kowalchuk, C. M.; Huang, Y.; Corrigan, J. F. *Chem. Commun.* **2000**, 1811. (b) Kowalchuk, C. M.; Huang, Y.; Corrigan, J. F. *Stud. Surf. Sci. Catal.* **2000**, *129*, 303.

(36) Peerson, O. B.; Wu, X.; Kustanovich, I.; Smith, S. O. *J. Magn. Reson., Ser. A* **1993**, *104* (3), 334.

(37) Bennett, A. E.; Rienstra, C. M.; Auger, M.; Lakshme, K. V.; Griffen, R. G. *J. Chem. Phys.* **1995**, *103*, 6951.

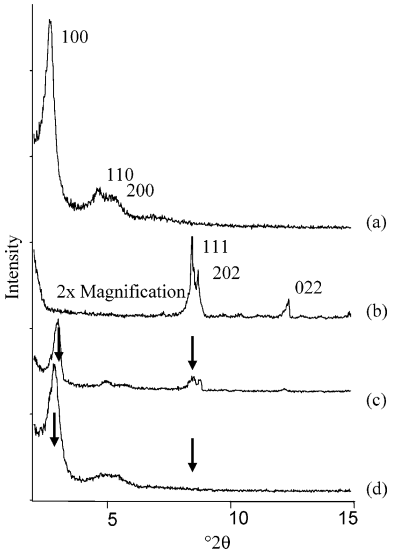


**Figure 1.** PXRD patterns 2−15° 2$\theta$ (all intensities normalized to the $d_{100}$ diffraction of MCM-41: (a) calcined MCM-41, $a_o$ 4.44 nm, $d_{100}$ 3.84 nm; (b) **1**; (c) I (**1**/MCM-41, 70 °C, $10^{-3}$ Torr), $a_o$ 3.94 nm, $d_{100}$ 3.41 nm; (d) II (**1**/MCM-41, 110 °C, $10^{-3}$ Torr), $a_o$ 4.21 nm, $d_{100}$ 3.65 nm.

element detection capability coupled to a Hitachi S-4500 SEM (scanning electron microscope). A 20 kV electron beam rastered over 100 $\mu$m × 100 $\mu$m areas was used to obtain semiquantitative analysis with the manufacturer's standardless software. Chemical analysis was performed by Chemisar Laboratories, Guelph, Canada.

The samples for the TEM characterization were obtained by dispersing the solid material with ethanol in an ultrasonic bath. The diluted dispersion was brought on carbon-coated copper-grids and investigated after evaporation of the ethanol in a FEI CM 200 FEG transmission electron microscope with a Super-Twin-Lens at an accelerating voltage of 200 keV (Cs = 1.2 mm, Cc = 1.2 mm, giving a point-resolution of 0.24 nm).

UV−vis diffuse reflectance measurements were performed on a Varian Cary Bio 100 spectrometer with a Varian diffuse reflectance attachment. Scan rates of 600 nm/min and a sweep width from 700 to 200 nm were utilized.

## Results and Discussion

The PXRD pattern of prepared MCM-41 (Figure 1a) has the characteristic $h_{100}$ reflection indexed from a hexagonal unit cell.[15] This corresponds to a $d$ spacing of 3.84 nm with a calculated pore size ($a_o = 2d_{100}/3^{1/2}$) of 4.4 nm. Subtracting 0.7 nm from this, resulting from the diameter of the pore wall as calculated from nitrogen adsorption, provides a pore size value of 3.7 nm. Second-order reflections ($h_{110}$, $h_{200}$) are also observed, which suggest high quality MCM-41 with long length channels. Intensities of all PXRD patterns are normalized with respect to the intensity of the $h_{100}$ reflection of MCM-41. The experimental PXRD pattern of **1** (Figure 1b) consists of three strong reflections. The calculated powder pattern of **1** (not shown) is identical to that observed in Figure 1b. The diffractions of **1** do not overlap with the reflections of MCM-41, and thus, crystalline **1** and MCM-41 integrity may be simultaneously probed. The cluster diameter from the edges of the stabilizing sphere is calculated to be 1.5 nm from the single-crystal data.[9] Thus, the pore size of MCM-41 is large enough to accommodate cluster **1**. The PXRD pattern of the sample obtained by mixing **1** and

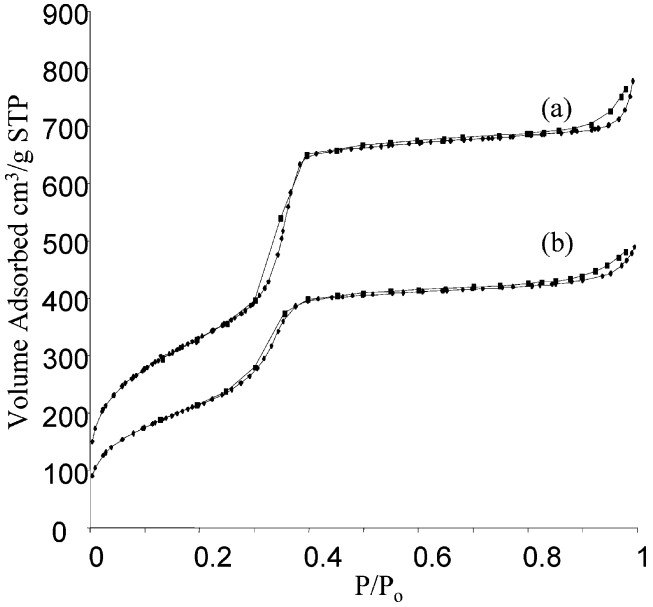


**Figure 2.** Nitrogen adsorption−desorption isotherms (diamonds, adsorption; squares, desorption): (a) MCM-41; (b) II (**1**/MCM-41, 110 °C, $10^{-3}$ Torr).

MCM-41 at 70 °C under a dynamic reduced pressure of $10^{-3}$ Torr (I) consists of the diffractions due to both pure crystalline **1** and MCM-41 indicating that some **1** still exists as crystallites (Figure 1c). Upon mixing **1** and MCM-41 at 110 °C, $10^{-3}$ Torr static vacuum (II) (Figure 1d) only the diffractions due to the MCM-41 are observed. The intensity of the $d_{100}$ peak decreased, and its peak position is also shifted to higher 2$\theta$ values ($\Delta d_{100} = 0.19$ nm, $\Delta a_o d_{100} = 0.23$ nm). It appears that the MCM-41 framework remains intact during impregnation at 110 °C and that **1** is distributed in the pores with no long range ordering. A decrease in intensity of the $h_{100}$ reflection observed upon loading **1** into the pores may be attributed to "contrast matching" between the amorphous silica pore walls and **1** distributed in the pores. This is consistent with loading electron rich materials into the channels of MCM-41.[38] The shift of the $d_{100}$ peak to higher 2$\theta$ suggests that the pore diameter has become slightly smaller with the impregnation of **1**.

The nitrogen adsorption/desorption isotherms of calcined MCM-41 (Figure 2a) display distinct capillary condensation and a type IV isotherm.[39,40] At low pressures ($P/P_o < 0.3$) the adsorption increases linearly with pressure. This region results from single and multilayer coverage on the exterior and interior pores of the MCM-41 framework.[41] In the region between $P/P_o$ 0.3−0.4 the amount of $N_2$ adsorbed increases dramatically corresponding to nitrogen filling the mesopores. At high relative pressures ($P/P_o > 0.9$) another linear increase is observed, a result of multilayer coverage on the surface.[41]

(38) Marler, B.; Oberhangemann, U.; Vortmann, S. Gies, H. *Microporous Mater.* **1996**, *6*, 375.
(39) Branton, P. J.; Hall, P. G.; Sing, K. S. *J. Chem. Soc., Chem. Commun.* **1993**, 1257.
(40) Sing, K. S. W.; Everett, D. H.; Haul, R. A. W.; Moscou, L.; Pierotti, R. A.; Rouquérol, J.; Siemieniewska, T. *Pure Appl. Chem.* **1985**, *57*, 603.
(41) Gregg, S. J.; Sing, K. S. W. *Adsorption, Surface Area and Porosity*, 2nd ed.; Academic Press: Toronto, 1982.

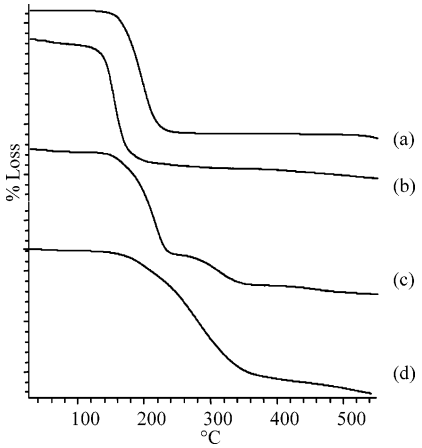


**Figure 3.** TGA curves, 25−550 °C, 10 °C/min: (a) **1**; (b) III (**1**/silicalite-1, 70 °C, $10^{-3}$ Torr); (c) I (**1**/MCM-41, 70 °C, $10^{-3}$ Torr); (d) II (**1**/MCM-41, 110 °C, $10^{-3}$ Torr).

The BET surface area for pure MCM-41 is calculated as 1214 $m^2/g$, and the average pore diameter (4V/A from BET) is 3.7 nm. Upon impregnation of MCM-41 with **1** (II, 12 wt %) (Figure 2b) the BET surface area decreases by 34% to 800 $m^2/g$ with retention of the type IV isotherm. The inflection point of the capillary condensation becomes less sharp and shifts to lower relative pressures, which is consistent with slightly smaller mesopores, confirming the PXRD data. The BJH adsorption pore volume decreases by 37% for the loaded sample II, consistent with a pore diameter (4V/A(BET)) decrease from 3.7 nm for calcined MCM-41 to 3.5 nm for II. These changes are a consequence of impregnating high molecular weight **1** into the pores. Since no significant lattice contraction was observed from the PXRD studies and the characteristic diffractions of the MCM-41 are still present, these observed isotherm changes must be due to occluded **1**.

Pure **1** is yellow in the crystalline state, and thermal decomposition (as monitored by TGA) proceeds with a single step of 70.5 wt % weight loss (Figure 3a) composed of two endothermic decompositions as determined by SDTA (not shown). The residual black powder is identified as $Cu_2Te$ as determined by PXRD. The observed weight loss during thermolysis corresponds to the loss of $PPh_2Et$ and $TePh_2$ as determined by GC/MS analysis. Complete elimination of these two species from **1** in a 5:3 ratio results in a calculated weight loss of 71.5%. The stability of solid **1** in air has been demonstrated, as crystals of **1** ground into a fine powder and left under atmospheric conditions for a period of 24 h exhibit a TGA curve identical to that observed in Figure 3a.

Silicalite-1 is a zeolite containing two orthogonal channel systems with pore diameters of about 0.53 nm, much too small to accommodate cluster **1**. The TGA curve (Figure 3b) of **1**/silicalite-1 (III) looks very similar to that of pure **1**, indicating that **1** only interacts weakly with the outer surface of the zeolite. The onset temperature for decomposition decreases slightly to 125 °C; however, the decomposition still proceeds in a single step. The slight decrease in the onset temperature is likely a result of diluting the crystals on the silicalite-1 external surface instead of **1** acting as a bulk crystalline material.

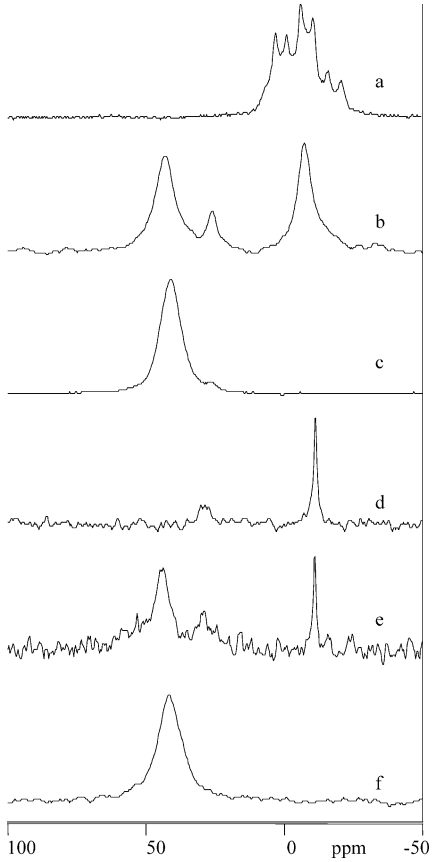


**Figure 4.** $^{31}P$ CP MAS NMR spectra: (a) **1**; (b) II (**1**/MCM-41, 110 °C, $10^{-3}$ Torr); (c) II separate preparation; (d) IV ($PPh_2Et$/MCM-41, 110 °C, $10^{-3}$ Torr); (e) IV+$O_2$; (f) V ($Ph_2EtP{=}O$/MCM-41, 110 °C, $10^{-3}$ Torr).

The **1**/MCM-41 sample I exhibits a new decomposition curve with an onset temperature of 250 °C (Figure 3c). The first low temperature decomposition starting at 135 °C is due to the cluster **1** located outside the channels of MCM-41 matched to small crystallites of pure **1**, and the higher temperature weight loss may be due to the decomposition of **1** inside the MCM-41 channels. For samples of II only the high temperature decomposition is present where **1** has been loaded into the pores of MCM-41 (Figure 3d). A maximum **1**/MCM-41 mixing ratio of 33 wt % and heating temperature of 110 °C provides the best loading percentages as determined by TGA. The PXRD, nitrogen adsorption, and TGA results suggest that **1** is impregnated into MCM-41 with no long range ordering.

To obtain the information on the local environments of **1** inside MCM-41 we carried out $^{31}P$ CP MAS NMR experiments. Figure 4a shows the $^{31}P$ CP MAS NMR spectrum of pure **1**, which has two overlapping quartets. The observed quartets are due to $^{31}P-^{63/65}Cu$ ($I = {}^3/_2$) $J$ coupling. The coupling constants are 1−1.5 kHz, which are consistent with previously reported values.[42] The free cluster **1** has three chemically nonequivalent P sites. In the solid state all five phosphorus centers are crystallographically nonequivalent.[9]

(42) (a) Olivieri, A. *J. Am. Chem. Soc.* **1992**, *114*, 5758. (b) Kolbert, A. C.; de Groot, H. J. M.; van der Putten, D.; Brom, H. B.; de Jongh, L. J.; Schmid, G.; Krautscheid, H.; Fenske, D. *Z. Phys. D* **1993**, *26*, 24. (c) Kroeker, S.; Hanna, J. V.; Wasylishen, R. E.; Ainscough, E. W.; Brodie, A. M. *J. Magn. Reson.* **1998**, *135*, 208.

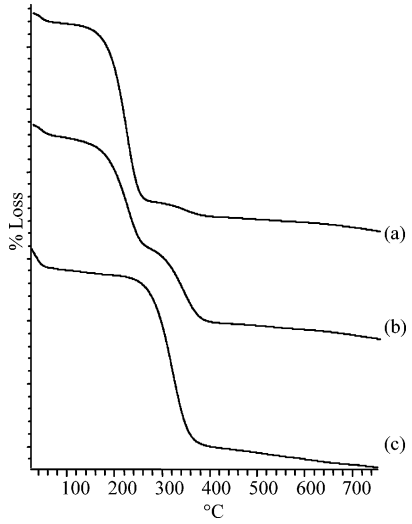


**Figure 5.** TGA curves 25−750 °C, 10 °C/min of organo phosphine containing compounds/MCM-41: (a) IV ($PPh_2Et$/MCM-41, 110 °C, $10^{-3}$ Torr); (b) IV+$O_2$; (c) V ($Ph_2EtP{=}O$/MCM-41, 110 °C, $10^{-3}$ Torr).

As shown in Figure 4a, two of them are resolved in the solid state with isotropic shift values being −3 and −19 ppm. In $C_6D_6$ only a very weak $^{31}P$ peak is observed at −10 ppm (spectrum not shown), and this resonance is broad ($\Delta\nu_{1/2}$ = 100 Hz). If **1** was to remain intact during impregnation, a single peak would be expected, centered at around −10 ppm similar to pure **1** in solution. In the $^{31}P$ CP MAS NMR spectrum of sample II, however, three peaks were observed at 42, 27, and −9 ppm (Figure 4b). The peak at 42 ppm has a wide spinning sideband pattern when spinning at 4 kHz resulting from a large chemical shift anisotropy (spectrum not shown). The peak at −9 ppm can be attributed to either cluster bound phosphine ligands or free phosphine (Figure 4d). The intensities of the peaks at 42 and −9 ppm vary from sample to sample. For example, in another sample prepared separately in the same manner a different $^{31}P$ CP MAS NMR spectrum is observed. It contains only two peaks at 42 and 27 ppm, and the peak at −9 is absent (Figure 4c). The full width at half-height maximum (fwhh) for samples of II which display the peak centered at −9 ppm is 780 Hz, with no resolved $^{31}P-^{63/65}Cu$ $J$ coupling. Although this $J$ value is much smaller than those observed for crystalline cluster **1**, it is broader than that observed for free $PPh_2Et$ in MCM-41 (IV) (225 Hz). The apparent lack of coupling suggests a nonordered or solution type environment. To determine the origin of the peaks at 42 and 27 ppm free phosphine ($PPh_2Et$) or the related phosphine oxide was directly loaded into MCM-41 and $^{31}P$ CP MAS NMR spectra and TGA curves were obtained. The $^{31}P$ CP MAS NMR spectrum of $PPh_2Et$/MCM-41 (IV) has a very strong peak at −9 ppm and a very weak peak at 27 ppm (Figure 4d). Both of these peaks are present in II. The strong peak at −9 ppm is very close to the solution $^{31}P$ NMR shift of $PPh_2Et$ (−10.8 ppm); therefore, this peak is assigned to the physisorbed phosphine. The TGA curve of IV has two decompositions (Figure 5a). The first has an onset of 130 °C, and the second begins at 290 °C, which overlaps with the high temperature decomposition of II (Figure 3d). The first mass loss is attributed to physiosorbed phosphine in the MCM-41 channels, consistent with the NMR peak observed at −9 ppm. The second decomposition at higher temperature correlates to the NMR peak at 27 ppm. The peak at 27 ppm has previously been observed for $PPh_2Et$ and attributed to a pentacoordinated P(V) nucleus of an oxyphosphorane on a silica surface.[43] The formation of this species is consistent with the higher TGA decomposition temperature observed.

**Scheme 1.** Oxidation of $PPh_2Et$ to $Ph_2EtP{=}O$[a]

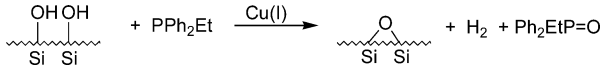


[a] See text.

Exposing IV to atmospheric oxygen for 11 h results in a $^{31}P$ CP MAS NMR spectrum (Figure 4e) containing a new peak at 42 ppm in addition to the peaks at 27 and −9 ppm. The peak centered at 42 ppm is also observed in samples of II. TGA of IV exposed to $O_2$ illustrates a new high temperature mass loss ($T$ = 270 °C) (Figure 5b) with the first loss now decreased in magnitude. The high temperature loss overlaps with the decomposition of II (T = 180 °C) (Figure 3e). The total mass loss increases from 15.5 wt % (Figure 5a) for IV to 16.6 wt % (Figure 5b) for the oxygen-exposed sample and can be interpreted to arise from the oxidation of the $PPh_2Et$ to $Ph_2EtP{=}O$. This conversion to the phosphine oxide was confirmed directly by loading $Ph_2EtP{=}O$ into MCM-41 to form V, for which there is a single peak observed in the $^{31}P$ CP MAS NMR spectrum at 42 ppm (Figure 4f). In the TGA trace of V a single mass loss occurs at 215 °C. This overlaps with the higher temperature mass loss for samples of IV + $O_2$ and is also observed for samples of II (Figure 5c). Loading of $Ph_2EtP{=}O$ into MCM-41 provides evidence that there is oxidation taking place when IV is exposed to atmospheric oxygen. The preparation of II, however, was under a strict inert atmosphere, and therefore the oxidation is not due to the presence of $O_2$. We suggest that the formation of $Ph_2EtP{=}O$ may occur catalytically due to the presence of Cu(I), which is a weak oxidation catalyst[44] according to Scheme 1. To verify the proposed mechanism we analyzed the gas evolved during the loading of **1** into MCM-41, and the formation of $H_2$ was confirmed via mass spectrometric analysis.

Cluster **1** inside the channels cannot be washed out of the pores of MCM-41 with organic solvents. For instance **1** has a solubility of greater than 200 mg in 5 mL of THF; however, when II is washed with THF on a Hirsch funnel, the loading remains unchanged as determined by TGA. Thus after the loss of the phosphine shell, the metal core of **1** must be attracted to the pore walls. It has been observed previously that bimetallic copper−ruthenium clusters coordinate to the

(43) Blümel, J. *Inorg. Chem.* **1994**, *33*, 5050.
(44) (a) Malkov, A. V.; Bella, M.; Langer, V.; Kocovsky, P. *Org. Lett.* **2000**, *2*, 3047. (b) Ohta, T.; Tachiyama, T.; Yoshizawa, K.; Yamabe, T.; Uchida, T.; Kitagawa, T. *Inorg. Chem.* **2000**, *39*, 4358. (c) Gupta, R.; Mukherjee, R. *Tetrahedron Lett.* **2000**, *41*, 7763. (d) Lee, W.-S.; Kwong, H.-L.; Chan, H.-L.; Choi, W.-W.; Ng, L.-Y. *Tetrahedron: Asymmetry* **2001**, *12*, 1007.

hydroxyl groups in the pores of MCM-41,[45] and computational studies also suggest that small monometallic copper clusters may bind through these hydroxyl linkages.[46] On the basis of the above discussion we suggest the following: during the impregnation process to form II, **1** has (partially or completely) lost the protective phosphine shell; the resulting "$Cu_6(TePh)_6$" core may be stabilized inside the MCM-41 via the interaction with the hydroxyl groups bound to the pore wall; and the free phosphine ligands displaced from **1** further undergo oxidation to form $Ph_2EtP{=}O$.

TEM measurements (200 keV) of II (20 wt %) were obtained (Figure 6a). This view, parallel to the pores, illustrates a network that is maintained during sample preparation, consistent with PXRD data. The actual cluster cores are unfortunately not resolved even though the photograph is obtained at maximum magnification. There is no evidence, however, of bulk cluster material located on the surface of the MCM-41. This further supports the PXRD and nitrogen adsorption evidence of **1** being impregnated inside MCM-41 at 110 °C.

EDX spectra of a sample of loaded **1**/MCM-41 (9 wt % as determined by TGA) indicate approximate ratios of 1.0:1.0 for Cu:Te, 0.8:1.0 for P:Cu, and 14.2:1.0 for Si:Cu. These values are in agreement with those obtained from chemical analysis of the same samples (3.2 wt % Cu and 5.7 wt %Te).

Thermolysis of loaded **1**/MCM-41 complexes should provide $Cu_2Te$ nanoclusters of the size regime less than the pore diameter. PXRD patterns of as prepared MCM-41 (Figure 7a) and II (12 wt %) (Figure 7b) display only an amorphous halo in the range of 20−35° 2$\theta$, consistent with the MCM-41 framework only being ordered in the direction parallel to the pores. A sample of II heated to 550 °C and annealed for 30 min at this temperature displays (Figure 7c) additional diffractions at higher angles. From the *d* spacings of these reflections the pattern may be indexed to orthorhombic $Cu_{0.64}Te_{0.36}$.[47] Heating the sample of II to 750 °C and annealing at this temperature results in the presence of indices assigned to a second orthorhombic phase of $Cu_{0.64}$-$Te_{0.36}$ (Figure 7d).[47] Miller indices were previously assigned to the PXRD diffractions,[47] no directional dependence was observed for our patterns corresponding to changes in peak line width suggesting that nanoparticles are formed versus nanowires. For both the 550 and 750 °C annealed samples low angle diffractions of MCM-41 are maintained. Annealing at 950 °C produces a pattern (Figure 7e) corresponding to $Cu_{0.64}Te_{0.36}$ in its high temperature phase, which crystallizes with a hexagonal habit.[47] The diffractions of $Cu_2Te$ sharpen and the line width is observed to decrease as compared to the 550 and 750 °C thermal treatment. These changes are due to the fact that the silicon framework decomposes when heated at 950 °C, as indicated by the disappearance of the characteristic reflections of MCM-41 at low angles.

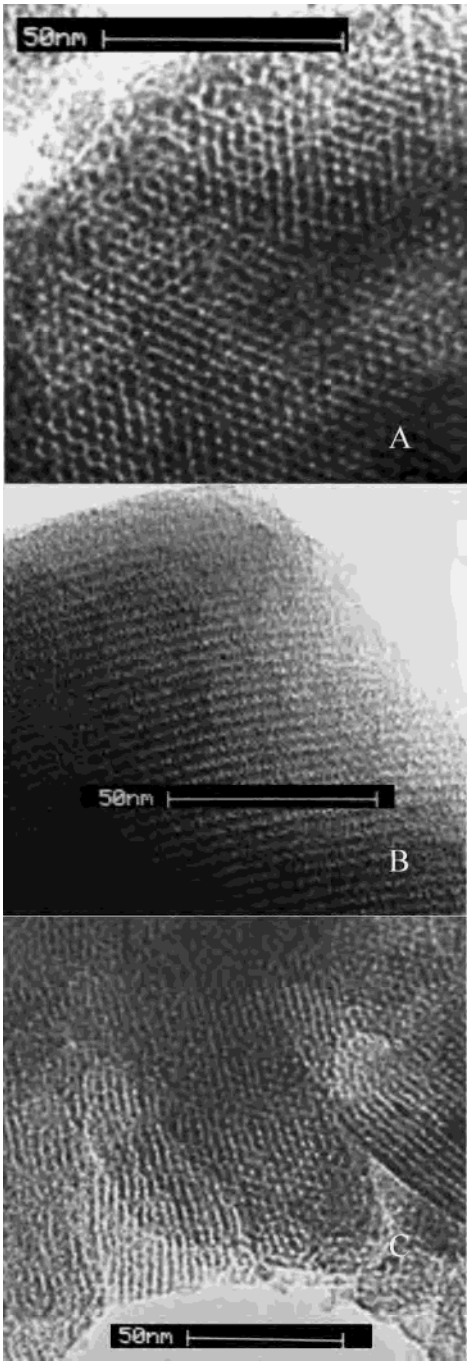


**Figure 6.** TEM images at 220 keV: (a) II (**1**/MCM-41, 110 °C, $10^{-3}$ Torr) parallel to the pore network; (b) annealed II at 550 °C perpendicular to the pores; (c) photolyzed II perpendicular to the pores.

A TEM image of the thermolyzed material annealed at 550 °C (20 wt % II) (Figure 6b) illustrates the apparent distortion of the silicate walls perpendicular to the pores. This may be due to condensed copper telluride in the channels. The TEM images provide evidence of framework integrity as observed in II (Figure 1) even though this sample has been heated to 550 °C. No observable condensed copper telluride is visible on the outside surface of the MCM-41.

It has been reported previously that solutions of **1** in benzene gradually darken upon irradiation forming the

(45) (a) Shephard, D. S.; Maschmeyer, T.; Sankar, G.; Thomas, J. M.; Ozkaya, D.; Johnson, B. F. G.; Raja, R.; Oldroyd, R. D.; Bell, G. B. *Chem. Eur. J.* **1998**, *4*, 1214. (b) Bromley, S. T.; Sankar, G.; Catlow, C. R. A.; Thomas, J. M.; Maschmeyer, T. *Microporous Mesoporous Mater.* **2001**, *44*−*45*, 395.
(46) Lopez, N.; Illas, F.; Pacchioni, G. *J. Phys. Chem. B* **1999**, *103*, 1712.
(47) Blacknik, R.; Lasocke, M.; Walbrecht, U. *J. Solid State Chem.* **1983**, *48*, 431.

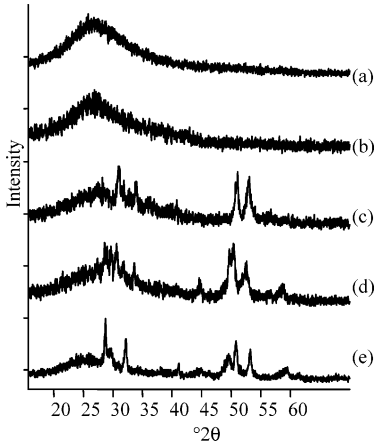


**Figure 7.** High angle PXRD of thermolyzed/annealed complexes: (a) MCM-41 (calcined); (b) II (**1**/MCM-41, 110 °C, $10^{-3}$ Torr) as-synthesized; (c) II annealed at 550 °C; (d) II annealed at 750 °C; (e) II annealed at 950 °C.

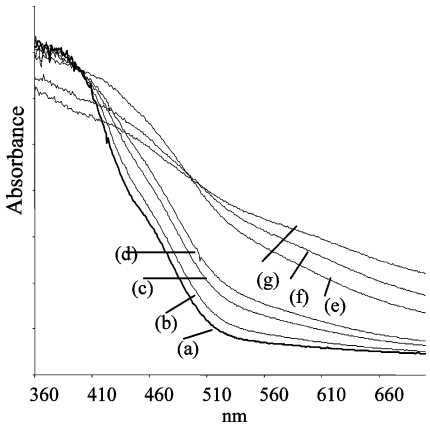


**Figure 8.** UV−vis DR time-resolved spectra of **1** obtained by applying the Kubelka−Munk function: (a) 0 h; (b) 10 min; (c) 20 min; (d) 30 min; (e) 120 min; (f) 240 min; (g) 480 min.

condensed cluster $[Cu_{50}(TePh)_{20}Te_{17}(PEtPh_2)_8][PEtPh_3]_4$ by ejection of $TePh_2$ and phosphine moieties.[9] The solution UV−vis spectrum of **1** contains two transitions, $\lambda_{max} = 287$ and 397 nm. The high energy absorption is assigned to $\pi-\pi^*$ transitions of the phenyl rings while the transition at $\lambda_{max} =$ 397 nm is assigned to the tellurolate-to-copper ligand to metal charge transfer (LMCT) band.[9,48] The solid state UV−vis diffuse reflectance spectrum of **1** has an onset of absorption at $\lambda = 550$ nm, with a partially resolved shoulder peak at 450 nm (Figure 8a). Upon irradiating **1** in benzene the bands at 287 and 397 nm are no longer observed. In the solid state, photolyzed **1** begins to absorb strongly at longer and longer wavelength as the irradiation time increases. After irradiating for 480 min a highly absorbing, featureless spectrum is obtained (Figure 8g). This can be explained as promoting random condensation by ejection of $TePh_2$ and $PPh_2Et$ from **1**. The ejection of $PPh_2Et$ and $TePh_2$ is confirmed by photolysis of suspensions of **1** in hexane and subsequent GC/MS analysis of the mother liquor. The UV−vis diffuse reflectance spectrum of II (12 wt %) consists of an absorption band at 350 nm much like the one observed in the solution spectrum of **1**. The presence of the band at 350 nm supports the idea that the metal cluster core is largely retained upon impregnation despite the (partial or complete) loss of the phosphine shell. Upon photolysis the disappearance of the band at 350 nm occurs after 30 min with no further change up to 180 min (UV−vis DR spectra available as Supporting Information). The condensation, therefore, only proceeds until no further $TePh_2$ moieties are ejected. Formation of $TePh_2$ is observed from slurries of II in hexane by GC/MS analysis of the mother liquor. There is no evidence however of $PPh_2Et$ being ejected from II when photolyzed as a slurry. The $PPh_2Et$ ligands may have been completely converted to $Ph_2EtP{=}O$ and coordinate to weakly acidic hydroxyl groups inside the pores. Although it is not anticipated that condensation reactions in the solid will be as selective as those in benzene to form $[Cu_{50}(TePh)_{20}Te_{17}(PEtPh_2)_8][PEtPh_3]_4$ from **1**, condensation processes are nonetheless occurring and must be limited to the specific size dimensions of the pore. These reactions proceed producing size restricted cluster particles, with continued irradiation having no noticeable effect on the absorption profiles of these samples.

A TEM image for the photocondensed material perpendicular to the pore direction is illustrated in Figure 6c (20 wt % II). There is no evidence of condensed material on the exterior of the MCM-41, providing additional evidence that the condensation must have taken place inside the pores.

## Conclusions

Cluster **1** may be impregnated into the pores of MCM-41 at 110 °C, $10^{-3}$ Torr. This proceeds with the partial loss of the phosphine shell and is further oxidized to form phosphine oxide. Thermal condensation of II produces $Cu_2Te$ in the pores. Photocondensation yields larger copper tellurium clusters within the space restricted framework.

**Acknowledgment.** We thank the Natural Sciences and Engineering Research Council (Canada), the Canada Foundation for Innovation, and the Academic Development Fund (UWO) for financial support. Mr. Sameen Zaidi and Prof. Sorab Rohani (UWO) are thanked for the nitrogen adsorption studies. Mrs. Li Huang is thanked for her assistance with the mass spectrometry ($H_2$) study. Dr. Chris W. Kirby is thanked for aid with the MAS NMR spectra.

**Supporting Information Available:** Time-resolved UV−vis DR spectra. This material is available free of charge via the Internet at http://pubs.acs.org.

IC0300868

(48) (a) Yam, V. W.-W.; Lo, K. K.-W. *Chem. Soc. Rev.* **1999**, *28*, 323. (b) Yam, V. W.-W.; Lam, C.-H.; Fung, W. K.-M.; Cheung, K.-K. *Inorg. Chem.* **2001**, *40*, 3435. (c) Yam, V. W.-W.; Lam, C.-H.; Cheung, K.-K. *Chem. Commun.* **2001**, 545.